Journal of Sound and Vibration (1997) **207**(5), 693–720

A HARMONIC FINITE ELEMENT FOR THE ANALYSIS OF FLEXURAL, TORSIONAL AND AXIAL ROTORDYNAMIC BEHAVIOR OF BLADE ARRAYS

G. GENTA

Department of Mechanics

AND

A. TONOLI

Department of Energetics, *Politecnico di Torino*, *Corso Duca degli Abruzzi* 24, 10129 *Torino*, *Italy*

(*Received* 5 *February* 1997, *and in final form* 2 *June* 1997)

The aim of this paper is to develop the formulation of a finite element for the study of the axial, torsional and flexural dynamic behavior of a rotating array of blades taking into account the gyroscopic effect and the centrifugal loadings. The displacements within the element are described in terms of superposition of the rigid body motion and the deflections relative to the rigid body configuration. A truncated Fourier's series has been adopted to approximate the dependence on tangential direction of the displacement field while polynomial shape functions are employed in the radial direction. Just the zero and one nodal diameter deflections have been considered in the Fourier series as they are the only ones coupled to the axial, torsional and flexural behavior of the disc–shaft system. The element equations of the motion are obtained using a complex co-ordinate formulation. Analytical solutions and experimental results have been compared to the results of the FEM model to test its accuracy.

1. INTRODUCTION

It is common practice in the rotordynamic study of rotors to neglect the flexibility of the disc-array of blades assemblies connected to them. The dynamic behavior of the disc assemblies is then analyzed in a separate step to determine if dangerous resonance conditions are met during operation. This approach corresponds to the implicit assumption that the disc–blade modes are decoupled to the dynamic behavior of the shaft. Even if this assumption leads to considerable simplification in the rotordynamic analysis, in the case when the shaft and the disc assemblies have natural frequencies close to each other a strong interaction can occur between them and the rigid body assumption becomes incorrect. The need of a model taking into account the interaction between shaft, disc and array of blades is emphasized in the case of rotors supported by active magnetic bearings. The coupling between axial and torsional degrees of freedom due to the presence of stagger and twist angles of the blades can lead the system to an instability due to the active control. In the case of actively controlled rotors, the risk of instability makes it of essential importance to take coupling effects into account in the design of the mechanical, electrical and control subsystems.

0022–460X/97/450693 + 28 $25.00/0/sv971147

A comprehensive survey article of the dynamic behavior of arrays of blades and their range of applicability is given by Leissa [1] considering both beam and plate/shells models. The differences occurring in the in-plane and out-of-plane vibrations induced by the rotational speed are pointed out along with the effects of the pretwist, the coupling between the bending and torsional degrees of freedom, and the effects of the shrouds.

To obtain a physical insight into the rotordynamic implications due to the flexibilities of disc and an array of blades attached to it, Crawley and Mokadam [2] and Chun and Lee [3] demonstrate that the stagger angle of the blades determines an inertial coupling between the in-plane and out-of-plane motion of the disc. In reference [2] evidence is given of the decoupling occurring between the motions involving two or more nodal diameters and the dynamic behavior of the shaft, so that just the zero and one nodal diameter are coupled to the dynamic of the shaft.

The equations of motion of a bladed disc are derived by Chun and Lee [3] in terms of the combination of the rigid body motion and the deflection of the disc and the array out of the rigid body configuration. No torsional and axial motions are considered and the solution of the equations of motion is carried out by means of admissible functions in the radial direction while a Fourier's series truncated at the first term has been employed to express the dependence on the tangential direction. Blade and shaft modes are shown to be strongly coupled in the case where their flexibility is comparable.

The interaction of flexible discs connected to flexible blades by means of compliant coupling is investigated by Tomioka *et al*. [4]. Springs are introduced between disc and blades to account for the flexibility of the coupling and between contiguous blades to account for the interaction between shrouds. A Ritz method is employed to approximate the dependence on radial co-ordinates of the unknown displacement field while the dependence from the angular location is expanded in a Fourier series. The study evidences a relation between the number of blades and the nodal diameters of the disc deflection. The influence of non-continuous shroud rings has been investigated both theoretically and experimentally by Zmitrowicz [5].

Even if the Ritz [2] and other assumed modes methods [3] can be helpful in obtaining a physical insight in the dynamic coupling due to the flexibility of the blades, their application in real-world configurations is very difficult, due to the complicated geometries usually adopted. The finite element method has been demonstrated to be more flexible to cope with these situations.

A number of papers has been written on the definition of finite elements suitable to the rotordynamic interaction due to the array of blades. Assuming the shaft as rigid, a two node Timoshenko type element has been developed by Kirkhope and Wilson [6] for the study of the dynamic behavior of the disc assembly. The degrees of freedom of the element include the axial, the tangential displacements of each blade cross-section and its twist angle. No coupling between bending and torsion is assumed (the flexural axis coincides with the centroidal axis). Since blade and disc are assumed to maintain common displacement and orientation at their interface, torsional modes of the blades are excited by the rim at the diametral nodes where the displacement is null but the orientation of the rim experiences a maximum variation.

A dynamic substructuring technique is used by Wildheim [7] to determine the blade–disc interaction. The displacement field within the system is expressed as the combination of a rigid body displacement field and the deflection out of it.

The strong excitation of the blade torsional modes occurring in helicopter rotor blades, led Magari *et al*. [8, 9] to the formulation of a beam finite element taking into account the distinction between centroid and shear centre of the sections. This analysis demonstrates a coupling between flexural and torsional modes of each blade.

The strong gyroscopic effects that can be induced on the rotor of a jet engine in the case of an aircraft manoeuver has been studied by Sakata *et al*. [10] by means of a model taking into account the interaction occurring between a flexible blade–disc assembly with a flexible shaft. Due to the decoupling demonstrated in [2], only the one nodal diameter modes are accounted for. In-plane, out-of-plane bending displacements and torsion of the blade are considered in the analysis.

While the approximation of the low aspect ratio blades as beams is usually successfully adopted for studying the interaction between shaft, disc and array of blades, it is not possible to predict local modes of the blades such as chordwise bending [1] and its interaction with the dynamic behavior of the disc. Distributed and lumped mass approaches are then adopted by Hsieh and Abel [11] to develop solid elements to be employed in the modelling of coupled disc–blade assemblies taking into account geometric non-linearities but not the coupling with the shaft and Coriolis effects due to rotation.

Low aspect ratio stub blades are studied by Omprakash and Ramamurti [12] by assuming the blades as shallow shells. The problem has been solved by means of the Rayleigh–Ritz method by exploiting the cyclic symmetry of the system.

The development of a finite element taking into account of the axial, flexural and torsional behavior of array of blades is carried out in the present paper also taking into account the coupling between axial and torsional behavior due to the stagger and pretwist angles. The blades are assumed to be clamped to the disc outer diameter and the interface is simulated by means of a disc–blade transition element that can be connected to a previously developed disc finite element [13]. The element matrices are obtained by means of a Lagrangian approach and the equations of motion are written in complex co-ordinates. The analytical solutions obtained in the case of a rotating pendulum and of a rotating blade connected to a rigid disc are used as an assessment of the accuracy of the results. Experimental results obtained on the rotor of a turbomolecular pump including several arrays of blades have also been compared with the predictions of the FEM model showing good agreement.

2. ELEMENT KINEMATICS

The main assumptions underlining the present analysis are that all the blades are equal, and are equally spaced along the outer diameter of the disc to which are connected the elastic and the inertial axes of the blades are aligned along a radial direction, the shear center and the centroid of each section are located at the same point of the section. The last assumption does not detract too much in the case of sections with a small camber of the airfoil such as in the case of turbomolecular pumps.

The number of blades must be such that the array is elastically and inertially axisymetric. Although the present formulation is developed with the assumption that the number of blades is even and higher than four, it can be adapted also for an odd number of blades provided that their number is high enough to make the asymmetries negligible. Figure 1 shows a blade cross-section taken perpendicularly to the radial direction. G indicates the centroid of the section, with u_1, u_2, u_3 its principal inertial axes and the reference frame with axes u, v, w along the radial, tangential and axial directions, an angle ψ due to the stagger and pretwist of the blade is defined between the axial direction w and axis u_2 of minimum inertia value.

Shear deformations and the rotational inertia of the cross-sections of the blades are considered to be negligible; this can be accepted in the case when the radius of gyration of the sections is small compared to the wavelength of the highest modes which are to be considered in the analysis. This assumption is usually acceptable in the case of the arrays

of blades employed for low pressure stages of gas turbines, compressors and high vacuum turbomolecular pumps while it can be questionable in the case of in-plane vibrations of the stub, low aspect ratio blades usually adopted for high pressure stages [1].

Due to the high number of blades usually included in an array, the uncorrelated motions of each individual blade do not affect the rotordynamic behavior of the shaft as they do not affect either the position of the centre of gravity or the orientation of the inertial axes of the array. Because this study addresses the motions influencing the rotordynamic behavior, only co-ordinated motions of the array are accounted for in the present analysis. Similarly to the case of the disc element [13], the array is then modelled as a two-dimensional object, all properties being concentrated along the radial inertial/elastic axes of each blade.

If both the blades and the interface with the shaft were rigid bodies, the orientation in space of the array would be dictated by the deformation of the shaft. During the deformation the reference plane of the array is assumed to maintain the same orientation in space of a rigid-body attached to the relevant shaft section, while the array, owing to its flexibility, exits this reference.

As in [13] and [14], the Lagrangian co-ordinates used to describe the rigid body motions of the array are: the displacement $\{\mathbf{C}\}$ of the geometrical center C of the shaft, angles Φ_x and Φ_y, indicating the orientation of the midplane and angle Φ_z accounting for the torsion. A further angle ϑ_i takes into account the angular location at time t of the undeformed configuration of the ith blade caused by the rotation of the shaft with angular speed ω. As the deformations of the array are described as deviations from the rigid body configuration, non-inertial terms can be foreseen in the equations of the motion.

By assuming that the cross-sections of each blade remain plane during the deformation, the dynamic behavior of the array can be described in terms of the location of the centroid of each section and of the rotations about the inertial axes.

Let u_i, v_i, w_i be the radial, tangential and axial displacement of the centroid P_i of a section of the ith blade taken at a radius r. Let $\{\mathbf{P}_i\}$ be the co-ordinates in an inertial reference of point P_i expressed as:

$$\{\mathbf{P}_i\} = \{\mathbf{C}\} + [\mathbf{R}](\{\mathbf{r}\} + \{\mathbf{s}_i\}), \tag{1}$$

where

$$[\mathbf{R}] = \prod_{i=1}^{4} [\mathbf{R}_i]; \qquad \{\mathbf{r}\} = \{r \quad 0 \quad 0\}^{\mathrm{T}}, \qquad \{\mathbf{s}\} = \{u \quad v \quad w\}^{\mathrm{T}}. \tag{2}$$

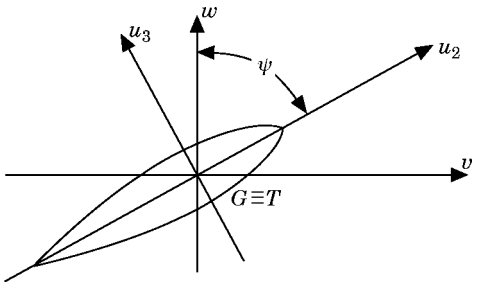

Figure 1. Cross-section of a blade; v, w = tangential and axial directions, u_2 = axis of minimum principal area moment of inertia u_3 = axis of maximum area moment of inertia.

The expressions of the rotation matrices $[\mathbf{R}_i]$ are reported in [14] as functions of angles $\Phi_{X'}$, Φ_y, Φ_z and ω. Due to the small values of angles Φ_i, $i = X', y, z$ the trigonometric functions within rotation matrices (2) (except for matrix $[\mathbf{R}_3]$) have been approximated by the first two terms of their Taylor series expansion. The displacement field expressed by equation (1) is very similar to that defined in [10] and in [3], the main difference being the inclusion of rotation Φ_z with the aim of modelling the torsional behavior of the rotor in addition to the axial and flexural ones. Unknown displacements u, v, w are functions of the radial location r of point P_i within the ith blade and of time t, while rigid body rotations $\Phi_{X'}$, Φ_y, Φ_z and displacements $\{\mathbf{C}\}$, are just depending on t. The absolute velocity $\{\dot{\mathbf{P}}\}$, is obtained as the time derivative of equation (1). The nomenclature is listed in the Appendix.

3. ELEMENT SHAPE FUNCTIONS

The displacements $u(r, \vartheta_i, z, t)$, $v(r, \vartheta_i, z, t)$, $w(r, \vartheta_i, z, t)$ have been approximated using shape functions of angle ϑ_i and radius r. The array of blades is discretized into annular elements of inner and outer radii r_i and r_o; a non-dimensional radial co-ordinate χ is defined as $\chi = (r - r_i)/\Delta r$ where $\Delta r = r_o - r_i$ is the radial thickness of the element. The area A of the cross-section of each blade, its area moments of inertia I_2, I_3 about the principal axes, and angle ψ are assumed to be linear functions of the non-dimensional radius χ within the element. Unknowns $u(\chi, \vartheta_i, z, t)$, $v(\chi, \vartheta_i, z, t)$, $w(\chi, \vartheta_i, z, t)$ are then approximated by means of a truncated Fourier's series expansion of the angular location ϑ_i.

$$
\begin{aligned}
u(\chi, \vartheta_i, t) &= u_x(\chi, t) \cos \vartheta_i + u_y(\chi, t) \sin \vartheta_i, \\
v(\chi, \vartheta_i, t) &= v_0(\chi, t) + v_y(\chi, t) \cos \vartheta_i - v_x(\chi, t) \sin \vartheta_i, \\
w(\chi, \vartheta_i, t) &= w_0(\chi, t) - w_y(\chi, t) \cos \vartheta_i + w_x(\chi, t) \sin \vartheta_i.
\end{aligned} \tag{3}
$$

The zero-order harmonics v_0 and w_0 account for the zero nodal diameter deformations of the array; they have been taken into account in the analysis as they describe the torsional and axial vibration of the array. The zero order term of the displacements u has been discarded as it is uncoupled with the axial, torsional and flexural behavior of the shaft. The first harmonic $u_{x,y}$, $v_{x,y}$, $w_{x,y}$ accounts for deformations with one nodal diameter; they have been included as describing a displacement field coupled to the flexural behavior. The higher order harmonics account for displacements that are not coupled to the axial, torsional and flexural behavior of the rotor, and have then been neglected [13].

Due to the orthogonality of trigonometric functions all harmonics contributions are decoupled with each other, the use of a truncated Fourier's series expansion instead of a complete one therefore does not lead to any major approximation in the retained terms [2].

As equations (3) approximate the unknown displacement field as a product of trigonometric functions of angle ϑ_i and unknown functions of χ and t, the truncated Fourier's series is equivalent to the implicit assumption of a shape function along the polar co-ordinate ϑ_i.

The subscripts of the coefficients in equations (3) and their signs have been adopted by considering that positive values of $u_x(\chi, t)$, $u_y(\chi, t)$ describe a displacement field leading to a displacement in the positive x and y directions of the centre of gravity of the array. The same holds for the coefficient function $v_y(\chi, t)$, while the displacement in $-x$ direction justifies the negative sign affecting $v_x(\chi, t)$. The subscripts and the signs in the last of equations (3) are set by taking into account that positive values of $w_x(\chi, t)$ and $w_y(\chi, t)$ determine a rotation of the principal axes of inertia of the array about the x- and $(-y)$-axes respectively.

Shape functions of the non-dimensional radial co-ordinate are then employed to approximate functions $u_{x,y}(\chi, t)$, $v_{x,y}(\chi, t)$ and $w_{x,y}(\chi, t)$ as a product of known functions of χ and a finite number of element Lagrangian co-ordinates:

$$\begin{aligned} v_0(\chi, t) &= [n_v(\chi)]\{q_{v0}(t)\}, \qquad w_0(\chi, t) = [n_w(\chi)]\{q_{w0}(t)\}, \\ u_x(\chi, t) &= [n_u(\chi)]\{q_{vx}(t)\}, \qquad u_y(\chi, t) = [n_u(\chi)]\{q_{uy}(t)\}, \\ v_x(\chi, t) &= [n_v(\chi)]\{q_{vx}(t)\}, \qquad v_y(\chi, t) = [n_v(\chi)]\{q_{vy}(t)\}, \\ w_x(\chi, t) &= [n_w(\chi)]\{q_{wx}(t)\}, \qquad w_y(\chi, t) = [n_w(\chi)]\{q_{wy}(t)\}. \end{aligned} \tag{4}$$

Linear functions are adopted for the displacements in the radial direction $u_{x,y}(\chi, t)$, while cubic polynomials for the tangential and the axial displacements $v_{x,y}(\chi, t)$ and $w_{x,y}(\chi, t)$:

$$[\mathbf{n}_u(\chi)] = [(1 - \chi)\chi] \quad [\mathbf{n}_v(\chi)] = [\mathbf{n}_w(\chi)] = [A \quad B \quad C \quad D], \tag{5}$$

where

$$\begin{aligned} A &= 2\chi^3 - 3\chi^2 + 1, \qquad C = \chi^2(2\chi - 3), \\ B &= (-\chi^3 + 2\chi^2 - \chi)\Delta r, \qquad D = \chi^2(1 - \chi)\Delta r. \end{aligned} \tag{6}$$

While in the case of a disc finite element [13] the elastic uncoupling between the deflections in-plane and out-of-plane of the disc justifies the use of shape functions of different orders, in the case of an array of blades the orientation ψ of the inertial axes leads to an elastic coupling between the deflections in-plane and out-of-plane of the disc. The adoption of shape functions of different order is then no longer justified. Even in the limiting cases of $\psi = 0, \pi/2$, when the two deflections are elastically uncoupled, the deflections in the plane and out of plane of the array are basically of the same type, thus suggesting the choice of identical shape functions.

The use of cubic shape functions requires the inclusion of the displacements and their radial derivatives $\beta_{v,wi}$ computed at the element inner and outer nodes ($j = 1, 2$) as element degrees of freedom. They are defined as:

$$\left.\begin{array}{ll} \beta_{wxj} = \partial v_{xj}/\partial r_j & \beta_{wyj} = \partial v_{yj}/\partial r_j \\ \beta_{vxj} = +\partial w_{xj}/\partial r_j, & \beta_{vyj} = +\partial w_{yj}/\partial r_j \end{array}\right\} \Rightarrow \text{with } j = 0, 1, 2 \tag{7}$$

subscript v and w indicate that the radial derivatives $\partial w_{x,y}/\partial r$ and $\partial v_{x,y}/\partial r$ can be thought as rotations about directions v and w respectively.

The set of Lagrangian co-ordinates employed to represent the displacements in the axial and in tangential directions (zero nodal diameters) of the array are then:

$$\{\mathbf{q}_{v0}\} = \{v_{01} \quad \beta_{w01} \quad v_{02} \quad \beta_{w02}\}^{\mathrm{T}}; \qquad \{\mathbf{q}_{w0}\} = \{w_{01} \quad \beta_{v01} \quad w_{02} \quad \beta_{v02}\}^{\mathrm{T}} \tag{8}$$

while those describing the deflections of the array coupled to the flexural behavior are (one nodal diameter):

$$\begin{aligned} \{\mathbf{q}_{ux}\} &= \{u_{x1} \quad u_{x2}\}^{\mathrm{T}}, \qquad \{\mathbf{q}_{uy}\} = \{u_{y1} \quad u_{y2}\}^{\mathrm{T}}, \\ \{\mathbf{q}_{vx}\} &= \{v_{x1} \quad \beta_{wx1} \quad v_{x2} \quad \beta_{wx2}\}^{\mathrm{T}}, \qquad \{\mathbf{q}_{vy}\} = \{v_{y1} \quad \beta_{wy1} \quad v_{y2} \quad \beta_{wy2}\}^{\mathrm{T}}, \\ \{\mathbf{q}_{wx}\} &= \{w_{x1} \quad \beta_{vx1} \quad w_{x2} \quad \beta_{vx2}\}^{\mathrm{T}}, \qquad \{\mathbf{q}_{wy}\} = \{w_{y1} \quad \beta_{vy1} \quad w_{y2} \quad \beta_{vy2}\}^{\mathrm{T}}. \end{aligned} \tag{9}$$

Substituting expressions (4) in (3) and then into equation (1), the configuration of the element at a given time is expressed in terms of known functions of the angular and radial locations and of a finite number of 34 Lagrangian co-ordinates.

The element is provided with three nodes: node 0 has six degrees of freedom: three translations of the central node $\{\mathbf{C}\}$ and three rigid body rotations:

$$\{q_0\} = \{X_C;\ Y_C;\ Z_C;\ \Phi_X;\ \Phi_y;\ \Phi_z;\}^{\mathrm{T}}. \tag{10}$$

The other two nodes are located at the inner and the outer radii, each of them is provided with 14 degrees of freedom describing the deflections listed in the vectors of equation (8) and (9).

4. EQUATIONS OF MOTION OF THE ELEMENT

The equations of motion of the element have been written from the expressions of the kinetic and the potential energies following a Lagrangian approach. Due to the assumption that the element is subject to small displacements, the expressions of the kinetic and potential energies have been computed by neglecting all contributions of orders higher than the second.

4.1. KINETIC ENERGY

The kinetic energy has been computed taking into account the contributions due to the rotational inertia of the cross-sections during the rigid body motions of the array while the contribution of the rotational inertia has been discarded when considering the deviations from the rigid body configuration. As in the case of the previously developed disc element [13], the flexural deformations of the blades are relevant only if the dimensions of the sections are small compared to the radial lengths. In the opposite case, if the sections are of a size comparable with the radial length, only rigid body motion needs to be accounted for.

Let $\{\dot{\mathbf{P}}_i\}_{XYZ}$ represent the velocity relative to the inertial reference $OXYZ$ of the centroid of the ith blade section at radius $r(\chi) = (r_1 + \Delta r\chi)$, the kinetic energy T is:

$$T = \tfrac{1}{2} \sum_{i=1}^{N} \int_0^1 \rho A(\chi) \{\dot{\mathbf{P}}_i\}^{\mathrm{T}} \{\dot{\mathbf{P}}_i\} \Delta r \, \mathrm{d}\chi, \tag{11}$$

where ρ is the mass density and $A(\chi)$ is the area of the section.

Expressing $\{\dot{\mathbf{P}}_i\}_{XYZ}$ as the time derivative of equation (1), the kinetic energy is expressed in terms of the degrees of freedom of node 0 included in matrix $[\mathbf{R}]$ and of the unknown displacement field $\{\mathbf{s}\}$. As this study is addressed to the definition of a linear finite element, the rotation matrix $[\mathbf{R}]$ and its time derivative have been approximated by the first two terms of the Taylor's series expansion in terms of the angular degrees of freedom of node 0. In this step the angular location ϑ_i of the ith blade has not been expanded being its value determined only by the angular speed and time t.

Indicating with subscripts 0, 1 and 2 the constant, first and second order contributions to the Taylor's series expansion, the velocity $\{\dot{\mathbf{P}}_i\}$ can be written in short-hand form as:

$$\{\dot{\mathbf{P}}_i\} = \{\dot{\mathbf{P}}_i\}_0 + \{\dot{\mathbf{P}}_i\}_1 + \{\dot{\mathbf{P}}_i\}_2. \tag{12}$$

Using the same notation to designate the different order contributions to matrices $[\mathbf{R}]$ and $[\dot{\mathbf{R}}]$, taking into account that vector $\{\mathbf{r}\}$ is a constant and that the unknown fields $\{\mathbf{s}\}$ and $\{\dot{\mathbf{s}}\}$ are of the first order in the degrees of freedom (9) of nodes 1 and 2, the three terms of equation (12) are given by:

$$\{\dot{\mathbf{P}}_i\}_0 = [\dot{\mathbf{R}}]_0\{\mathbf{r}\}, \qquad \{\dot{\mathbf{P}}_i\}_1 = \{\dot{\mathbf{C}}\} + [\dot{\mathbf{R}}]_1\{\mathbf{r}\} + [\dot{\mathbf{R}}]_0\{\mathbf{s}\} + [\mathbf{R}]_0\{\dot{\mathbf{s}}\},$$
$$\{\dot{\mathbf{P}}_i\}_2 = [\dot{\mathbf{R}}]_2\{\mathbf{r}\}_0 + [\dot{\mathbf{R}}]_1\{\mathbf{s}\} + [\dot{\mathbf{R}}]_1\{\dot{\mathbf{s}}\}. \tag{13}$$

Substituting equation (12) in equation (11), taking into account that the rotation matrix $[\mathbf{R}]_0$ is an identity matrix, and that $[\dot{\mathbf{R}}]_0$ is null, then neglecting all contributions of order higher than the second, the kinetic energy becomes:

$$T = T_0 + T_1 + T_2, \tag{14}$$

where

$$T_0 = \tfrac{1}{2} \sum_{i=1}^{N} \int_0^1 \rho A(\chi) \{\dot{\mathbf{P}}_i\}_0^{\mathrm{T}} \{\dot{\mathbf{P}}_i\}_0 \Delta r \, \mathrm{d}\chi,$$

$$T_1 = \tfrac{1}{2} \sum_{i=1}^{N} \int_0^1 \rho A(\chi) (\{\dot{\mathbf{P}}_i\}_0^{\mathrm{T}} \{\dot{\mathbf{P}}_i\}_1 + \{\dot{\mathbf{P}}_i\}_1^{\mathrm{T}} \{\dot{\mathbf{P}}_i\}_0) \Delta r \, \mathrm{d}\chi,$$

$$T_2 = \tfrac{1}{2} \sum_{i=1}^{N} \int_0^1 \rho A(\chi) (\{\dot{\mathbf{P}}_i\}_1^{\mathrm{T}} \{\dot{\mathbf{P}}_i\}_1 + \{\dot{\mathbf{P}}_i\}_0^{\mathrm{T}} \{\dot{\mathbf{P}}_i\}_2 + \{\dot{\mathbf{P}}_i\}_2^{T} \{\dot{\mathbf{P}}_i\}_0) \Delta r \, \mathrm{d}\chi. \tag{15}$$

As only the second order component T_2 needs to be taken into account in writing the Lagrange's equations as the zero and the first order contributions, T_0 and T_1 give way to null or constant terms in the element dynamic equations; the latter have then been discarded for the sake of simplifying the analytical work involved in their explicit computation.

The discretized expressions (3) and (4) are then substituted in T_2 to obtain the element kinetic energy in terms of its Lagrangian co-ordinates. In computing the time derivatives, angle ϑ_i must be considered as a function of time so that:

$$\mathrm{d}\vartheta_i / \mathrm{d}t = \omega. \tag{16}$$

In the case when the number of blades N is even, the orthogonality of the harmonics functions leads to a decoupling between the zero and the first harmonic contributions to the kinetic energy. The explicit computation of the kinetic energy of equation (15) shows a decoupling between the axial, torsional and flexural behavior. Similarly the first harmonic terms contributing to the in-plane displacements u, v and the out-of-plane ones w are decoupled. The kinetic energy can then be split into four independent contributions:

$$T = T_{axl} + T_{trs} + T_{inp} + T_{outp} \tag{17}$$

where the axial T_{axl}, torsional T_{trs}, in-plane T_{inp} and the out of plane T_{outp} contributions to the kinetic energy can be expressed as functions of the element degrees of freedom and of the shape functions:

$$\begin{aligned}
T_{axl} &= \tfrac{1}{2}(m\dot{Z}_0^2 + 2\dot{Z}_0[\mathbf{m}_{axl1}]\{\dot{\mathbf{q}}_{w0}\} + \{\dot{\mathbf{q}}_{w0}\}^{\mathrm{T}}[\mathbf{m}_{axl2}]\{\dot{\mathbf{q}}_{w0}\}),\\
T_{trs} &= \tfrac{1}{2}[J_p(\omega + \dot{\Phi}_z)^2 + 2(\omega + \dot{\Phi}_z)[\mathbf{m}_{trs1}]\{\dot{\mathbf{q}}_{v0}\} + \omega^2\{\mathbf{q}_{v0}\}^{\mathrm{T}}[\mathbf{m}_{trs2}]\{\mathbf{q}_{v0}\}\\
&\quad + \{\dot{\mathbf{q}}_{v0}\}^{\mathrm{T}}[\mathbf{m}_{trs2}]\{\dot{\mathbf{q}}_{v0}\}],\\
T_{inp} &= \tfrac{1}{2}[\omega^2(\{\mathbf{q}_{ux}\}^{\mathrm{T}}[\mathbf{m}_{inp1}]\{\mathbf{q}_{ux}\} + \{\mathbf{q}_{uy}\}^{\mathrm{T}}[\mathbf{m}_{inp1}]\{\mathbf{q}_{uy}\} + \{\mathbf{q}_{vx}\}^{\mathrm{T}}[\mathbf{m}_{inp2}]\{\mathbf{q}_{vx}\}\\
&\quad + \{\mathbf{q}_{vy}\}^{\mathrm{T}}[\mathbf{m}_{inp2}]\{\mathbf{q}_{vy}\} - 2\{\mathbf{q}_{ux}\}^{\mathrm{T}}[\mathbf{m}_{inp3}]\{\mathbf{q}_{vx}\} - 2\{\mathbf{q}_{uy}\}^{\mathrm{T}}[\mathbf{m}_{inp3}]\{\mathbf{q}_{vy}\})\\
&\quad + \omega(\{\mathbf{q}_{uy}\}^{\mathrm{T}}[\mathbf{m}_{inp1}]\{\dot{\mathbf{q}}_{ux}\} - \{\mathbf{q}_{vy}\}^{\mathrm{T}}[\mathbf{m}_{inp3}]^{\mathrm{T}}\{\dot{\mathbf{q}}_{ux}\} - \{\mathbf{q}_{ux}\}^{\mathrm{T}}[\mathbf{m}_{inp1}]\{\dot{\mathbf{q}}_{uy}\}\\
&\quad + \{\mathbf{q}_{vx}\}^{\mathrm{T}}[\mathbf{m}_{inp3}]\{\dot{\mathbf{q}}_{uy}\} - \{\mathbf{q}_{uy}\}^{\mathrm{T}}[\mathbf{m}_{inp3}]\{\dot{\mathbf{q}}_{vx}\} + \{\mathbf{q}_{vy}\}^{\mathrm{T}}[\mathbf{m}_{inp2}]\{\dot{\mathbf{q}}_{vx}\}\\
&\quad + \{\mathbf{q}_{ux}\}^{\mathrm{T}}[\mathbf{m}_{inp3}]\{\dot{\mathbf{q}}_{vy}\} - \{\mathbf{q}_{vx}\}^{\mathrm{T}}[\mathbf{m}_{inp2}]\{\dot{\mathbf{q}}_{vy}\}) + \tfrac{1}{2}\{\dot{\mathbf{q}}_{ux}\}^{\mathrm{T}}[\mathbf{m}_{inp1}]\{\dot{\mathbf{q}}_{ux}\}
\end{aligned}$$

$$+ \{\dot{\mathbf{q}}_{uy}\}^{\mathrm{T}}[\mathbf{m}_{inp1}]\{\dot{\mathbf{q}}_{uy}\} + \{\dot{\mathbf{q}}_{vx}\}^{\mathrm{T}}[\mathbf{m}_{inp2}]\{\dot{\mathbf{q}}_{vx}\} + \{\dot{\mathbf{q}}_{vy}\}^{\mathrm{T}}[\mathbf{m}_{inp2}]\{\dot{\mathbf{q}}_{vy}\}$$
$$+ \dot{X}_0[\mathbf{m}_{inp4}]\{\dot{\mathbf{q}}_{ux}\} + \dot{X}_0[\mathbf{m}_{inp5}]\{\dot{\mathbf{q}}_{vx}\} + m(\dot{X}_0^2 + Y_0^2)$$
$$+ \dot{Y}_0[\mathbf{m}_{inp4}]\{\dot{\mathbf{q}}_{uy}\} + \dot{Y}_0[\mathbf{m}_{inp3}]\{\dot{\mathbf{q}}_{vy}\}],$$

$$T_{outp} = \tfrac{1}{2}[\omega^2(\{\mathbf{q}_{wx}\}^{\mathrm{T}}[\mathbf{m}_{outp2}]\{\mathbf{q}_{wx}\} + \{\mathbf{q}_{wy}\}^{\mathrm{T}}[\mathbf{m}_{outp2}]\{\mathbf{q}_{wy}\}) + \omega(2J_p\Phi_y\dot{\Phi}_{X'}$$
$$+ 4\dot{\Phi}_{X'}[\mathbf{m}_{outp1}]\{\mathbf{q}_{wy}\} - 4\dot{\Phi}_y[\mathbf{m}_{outp1}]\{\mathbf{q}_{wx}\} + 2\{\mathbf{q}_{wy}\}^{\mathrm{T}}[\mathbf{m}_{outp2}]\{\dot{\mathbf{q}}_{wx}\}$$
$$- 2\{\mathbf{q}_{wx}\}^{\mathrm{T}}[\mathbf{m}_{outp2}]\{\dot{\mathbf{q}}_{wy}\}) + J_t(\dot{\Phi}_{x'}^2 + \Phi_y^2) + 2\dot{\Phi}_y[\mathbf{m}_{outp1}]\{\dot{\mathbf{q}}_{wx}\}$$
$$+ 2\dot{\Phi}_{X'}[\mathbf{m}_{outp1}]\{\dot{\mathbf{q}}_{wx}\} + \{\dot{\mathbf{q}}_{wx}\}^{\mathrm{T}}[\mathbf{m}_{outp2}]\{\dot{\mathbf{q}}_{wx}\} + \{\dot{\mathbf{q}}_{wy}\}^{\mathrm{T}}[\mathbf{m}_{outp2}]\{\dot{\mathbf{q}}_{wy}\}], \tag{18}$$

where m is the element mass, J_p its polar moment of inertia about the z-axis while J_t is its moment of inertia about one of the radial directions through the element center of mass. Matrices $[\mathbf{m}_{axli}]$, $[\mathbf{m}_{trsi}]$, $[\mathbf{m}_{inpi}]$ and $[\mathbf{m}_{outpi}]$ are given by integrals:

$$[\mathbf{m}_{axl1}] = N\int_{r_i}^{r_o}\rho A[n_w]\,dr = N\int_{r_i}^{r_o}\rho A[n_v]\,\mathrm{d}r,$$

$$[\mathbf{m}_{axl2}] = N\int_{r_i}^{r_o}\rho A[n_w]^{\mathrm{T}}[n_w]\,\mathrm{d}r = N\int_{r_i}^{r_o}\rho A[n_v]^{\mathrm{T}}[\eta_v]\,\mathrm{d}r,$$

$$[\mathbf{m}_{trs1}] = N\int_{r_i}^{r_o}\rho rA[n_w]\,\mathrm{d}r = N\int_{r_i}^{r_o}\rho rA[n_v]\,\mathrm{d}r,$$

$$[\mathbf{m}_{trs2}] = N\int_{r_i}^{r_o}\rho A[n_w]^{\mathrm{T}}[n_w]\,\mathrm{d}r = N\int_{r_i}^{r_o}\rho A[n_v]^{\mathrm{T}}[n_v]\,\mathrm{d}r,$$

$$[\mathbf{m}_{inp1}] = \frac{N}{2}\int_{r_i}^{r_o}\rho A[n_u]^{\mathrm{T}}[n_u]\,\mathrm{d}r,$$

$$[\mathbf{m}_{inp2}] = \frac{N}{2}\int_{r_i}^{r_o}\rho A[n_w]^{\mathrm{T}}[n_w]\,\mathrm{d}r = \frac{N}{2}\int_{r_i}^{r_o}\rho A[n_v]^{\mathrm{T}}[n_v]\,\mathrm{d}r,$$

$$[\mathbf{m}_{inp3}] = \frac{N}{2}\int_{r_i}^{r_o}\rho A[n_u]^{\mathrm{T}}[n_w]\,\mathrm{d}r = \frac{N}{2}\int_{r_i}^{r_o}\rho A[n_u]^{\mathrm{T}}[n_v]\,\mathrm{d}r,$$

$$[\mathbf{m}_{inp4}] = \frac{N}{2}\int_{r_i}^{r_o}\rho A[n_u]\,\mathrm{d}r$$

$$[\mathbf{m}_{inp5}] = \frac{N}{2}\int_{r_i}^{r_o}\rho A[n_w]\,\mathrm{d}r = \frac{N}{2}\int_{r_i}^{r_o}\rho A[n_v]\,\mathrm{d}r,$$

$$[\mathbf{m}_{outp1}] = \frac{N}{2}\int_{r_i}^{r_o}\rho rA[n_w]\,\mathrm{d}r = \frac{N}{2}\int_{r_i}^{r_o}\rho rA[n_v]\,\mathrm{d}r,$$

$$[\mathbf{m}_{outp2}] = \frac{N}{2}\int_{r_i}^{r_o}\rho A[n_w]^{\mathrm{T}}[n_w]\,\mathrm{d}r = \frac{N}{2}\int_{r_i}^{r_o}\rho A[n_v]^{\mathrm{T}}[n_v]\,\mathrm{d}r.$$

The choice of a non-inertial frame $Cxyz$ for the definition of the element Lagrangian co-ordinates makes the kinetic energy function of both the displacements and velocities. The expressions (18) and (19) are valid for an array of blades and those valid for a disc element [13] are nearly identical: this is due to the assumption that the blades are located at constant angular steps, that their number is even and that the rotational inertia of the sections is negligible compared to their mass. This last assumption is responsible of the decoupling between axial and torsional contributions to the kinetic energy even when the stagger angle $\psi \neq 0,\ \pi/2$.

4.2. POTENTIAL ENERGY

The potential energy of the element is due both to the elastic strain–stress nature of the material (U_e) and to the contribution usually referred to as the "geometric effect" (U_g). The latter accounts for the increase in the element stiffness due to the radial centrifugal force acting along the axis of each blade (centrifugal stiffening):

$$U = U_e + U_g \tag{20}$$

Due to the assumptions that the radial dimensions of each blade are large compared to its cross-sections and that its shear deformations are negligible, each blade can be considered as a Bernoulli's beam. With A indicating the area of the cross-section and I_2 and I_3 its area of moments of inertia about the principal axes u_2 and u_3 of Figure 1, the elastic energy U_e of the array is expressed as the sum of the contributions due to the radial extension of each blade and to the flexural deflections along the axes u_2 and u_3:

$$U_e = \tfrac{1}{2} \sum_{i=1}^{N} \int_0^1 E\left[\frac{A}{\Delta r}(s_1')^2 + \frac{1}{\Delta r^3}(I_2(s_2'')^2 + I_3(s_3'')^2)\right] \mathrm{d}\chi. \tag{21}$$

Prime ($'$) indicates the partial derivative relative to the non-dimensional radial co-ordinate χ and E is Young's modulus. The displacements s_1, s_2, s_3 along the inertial axes are linked to the axial, tangential and radial directions by means of angle ψ:

$$s_1 = u, \qquad s_2 = v\cos\psi + w\sin\psi, \qquad s_3 = w\cos\psi - v\sin\psi. \tag{22}$$

The expression of the elastic potential energy is obtained in terms of the element degrees of freedom by substituting the discretized displacements of equations (4) and (3) in equation (22) and finally in (21). In the case when angle ψ is such that the inertial axes 2 and 3 of the sections are not aligned with tangential and axial directions ($\psi \neq 0,\ \pm\pi/2$), the axial and torsional degrees of freedom are shown to be coupled in the potential energy contribution $U_{eaxltrs}$ while the in plane and out of plane degrees of freedom give way to contributions U_{einp}, U_{eoutp} which are decoupled regardless of the value of angle ψ:

$$U_e = U_{eaxltrs} + U_{einp} + U_{eoutp} \tag{23}$$

contributions $U_{eaxltrs}$, U_{einp} and U_{eoutp} are expressed in terms of the element degrees of freedom as:

$$U_{eaxltrs} = \tfrac{1}{2}(\{\mathbf{q}_{w0}\}^{\mathrm{T}}[\mathbf{k}_{eaxltrs1}]\{\mathbf{q}_{w0}\} + \{\mathbf{q}_{v0}\}^{\mathrm{T}}[\mathbf{k}_{eaxltrs2}]\{\mathbf{q}_{v0}\} + 2\{\mathbf{q}_{v0}\}^{\mathrm{T}}[\mathbf{k}_{eaxltrs3}]\{\mathbf{q}_{w0}\}),$$

$$U_{einp} = \tfrac{1}{2}(\{\mathbf{q}_{ux}\}^{\mathrm{T}}[\mathbf{k}_{einp1}]\{\mathbf{q}_{ux}\} + \{\mathbf{q}_{uy}\}^{\mathrm{T}}[\mathbf{k}_{einp1}]\{\mathbf{q}_{uy}\} + \{\mathbf{q}_{vx}\}^{\mathrm{T}}[\mathbf{k}_{einp2}]\{\mathbf{q}_{vx}\} + \{\mathbf{q}_{vy}\}^{\mathrm{T}}[\mathbf{k}_{einp2}]\{\mathbf{q}_{vy}\}),$$

$$U_{eoutp} = \tfrac{1}{2}(\{\mathbf{q}_{wx}\}^{\mathrm{T}}[\mathbf{k}_{eoutp}]\{\mathbf{q}_{wx}\} + \{\mathbf{q}_{wy}\}^{\mathrm{T}}[\mathbf{k}_{eoutp}]\{\mathbf{q}_{wy}\}). \tag{24}$$

Stiffness matrices $[\mathbf{k}_{ei}]$ are given as functions of the shape functions by the following integrals:

$$[\mathbf{k}_{eaxltrs1}] = \frac{N}{\Delta r^3}\int_0^1 EI_v[\mathbf{n}''_{v0}]^{\mathrm{T}}[\mathbf{n}''_{w0}]\,\mathrm{d}\chi, \qquad [\mathbf{k}_{eaxltrs2}] = \frac{N}{\Delta r^3}\int_0^1 EI_v[\mathbf{n}''_{v0}]^{\mathrm{T}}[\mathbf{n}''_{v0}]\,\mathrm{d}\chi,$$

$$[\mathbf{k}_{eaxltrs3}] = \frac{N}{\Delta r^3}\int_0^1 EI_{vw}[\mathbf{n}''_{v0}]^{\mathrm{T}}[\mathbf{n}''_{w0}]\,\mathrm{d}\chi, \qquad [\mathbf{k}_{einp1}] = \frac{N}{2\Delta r}\int_0^1 EA[\mathbf{n}'_u]^{\mathrm{T}}[\mathbf{n}'_u]\,\mathrm{d}\chi,$$

$$[\mathbf{k}_{einp2}] = \frac{N}{2\Delta r^3}\int_0^1 EI_w[\mathbf{n}''_v]^{\mathrm{T}}[\mathbf{n}''_v]\,\mathrm{d}\chi, \qquad [\mathbf{k}_{eoutp}] = \frac{N}{2\Delta r^3}\int_0^1 EI_v[\mathbf{n}''_w]^{\mathrm{T}}[\mathbf{n}''_w]\,\mathrm{d}\chi. \tag{25}$$

I_v, I_w are the area moments of inertia of a section relative to the tangential and the axial directions v and w of Figure 1. The area moment of inertia I_{vw} is responsible for the coupling between the axial and torsional degrees of freedom due to angle ψ. In the case where the principal inertial axes of all the blade sections are aligned with the tangential and axial directions, $I_{vw} = 0$ and the torsional and axial behaviors of the array become elastically decoupled.

Whenever a section is pushed out of its unperturbed location, the radial centrifugal pull acting on it originates a restoring force that tends to bring it back to the undeformed condition. The second contribution, U_g, to the potential energy of equation (20) is usually referred to as "geometric effect" and is caused by the centrifugal forces F_r that the portion of each blade extending from a given radius r to the tip r_o applies on the section at radius r. Assuming that the blades are free to expand radially at the tip, the thermal effects do not induce any radial load along the axis of the blades, the force F_r can then be expressed as:

$$F_r(r) = \omega^2\int_r^{r_o}\rho Ar\,\mathrm{d}r = \omega^2 P_{r\omega}(r) \tag{26}$$

where $P_{r\omega}(r)$ represents the radial force per unit rotational speed (kgm) of the portion of the blade from radius r to the tip. It is worth noting that the restoring force due to the centrifugal field is the only one acting in the case of the rotating pendulum shown in the example 6.1. The geometric contribution to the potential energy can be expressed as:

$$U_g = \frac{1}{2\Delta r}\sum_{i=1}^{N}\int_0^1 F_r(\chi)[v'^2 + w'^2]\,\mathrm{d}\chi. \tag{27}$$

Substituting the discretized displacements of equations (3) (4) into equation (27), the geometric term in the potential energy can be split into four independent contributions:

$$U_g = U_{gaxl} + U_{gtrs} + U_{ginp} + U_{poutp}, \tag{28}$$

where

$$U_{gaxl} = \tfrac{1}{2}\omega^2\{\mathbf{q}_{w0}\}^{\mathrm{T}}[\mathbf{k}_{gaxl\omega}]\{\mathbf{q}_{w0}\}, \qquad U_{gtrs} = \tfrac{1}{2}\omega^2\{\mathbf{q}_{v0}\}^{\mathrm{T}}[\mathbf{k}_{gtrs\omega}]\{\mathbf{q}_{v0}\},$$
$$U_{ginp} = \tfrac{1}{2}\omega^2(\{\mathbf{q}_{vx}\}^{\mathrm{T}}[\mathbf{k}_{ginp\omega}]\{\mathbf{q}_{vx}\} + \{\mathbf{q}_{vy}\}^{\mathrm{T}}[\mathbf{k}_{ginp\omega}]\{\mathbf{q}_{vy}\}),$$
$$U_{goutp} = \tfrac{1}{2}\omega^2(\{\mathbf{q}_{wx}\}^{\mathrm{T}}[\mathbf{k}_{goutp\omega}]\{\mathbf{q}_{wx}\} + \{\mathbf{q}_{wy}\}^{\mathrm{T}}[\mathbf{k}_{goutp\omega}]\{\mathbf{q}_{wy}\}). \tag{29}$$

As with the case of the kinetic energy of equation (17), no coupling is introduced because of the geometric term U_g between the torsional and the axial degrees of freedom. The geometric stiffness matrices $[\mathbf{k}_{gi\omega}]$ are given by the following integrals of the shape functions and of $P_{r\omega}$ of equation (26):

$$[\mathbf{k}_{gaxl\omega}] = \frac{2N}{\Delta r}\int_0^1 P_{r\omega}[\mathbf{n}'_{w0}]^{\mathrm{T}}[\mathbf{n}'_{w0}]\,\mathrm{d}\chi, \qquad [\mathbf{k}_{gtrs\omega}] = \frac{2N}{\Delta r}\int_0^1 P_{r\omega}[\mathbf{n}'_{v0}]^{\mathrm{T}}[\mathbf{n}'_{v0}]\,\mathrm{d}\chi,$$

$$[\mathbf{k}_{ginp\omega}] = \frac{N}{\Delta r}\int_0^1 P_{r\omega}[\mathbf{n}'_{t}]^{\mathrm{T}}[\mathbf{n}'_{v}]\,\mathrm{d}\chi, \qquad [\mathbf{k}_{goutp\omega}] = \frac{N}{\Delta r}\int_0^1 P_{r\omega}[\mathbf{n}'_{w}]^{\mathrm{T}}[\mathbf{n}'_{w}]\,\mathrm{d}\chi, \tag{30}$$

As the force F_r of equation (26) has no constant contributions due to thermal effects or shrink fit conditions, the geometric stiffness matrices always give a stiffening effect, at least in the case when the blades are connected to the rotor at the inner radius.

4.3. ELEMENT MATRICES

The Lagrangian function $L = T - U$ of the element is obtained from the kinetic energy of equation (17) and the potential energy of equation (20). As both the potential and kinetic energies show a decoupling between the in-plane and out-of-plane degrees of freedom, the in-plane and out-of-plane dynamic equations of the element will be decoupled between them while an angle $\psi \neq 0,\ \pi/2$, will determine a coupling between axial and torsional degrees of freedom. This coupling is due to the contribution $U_{eaxltrs}$ of equation (24). Although coupled with each other, the axial and torsional equations of motion will be decoupled to both in-plane and out-of-plane flexural degrees of freedom. It is then possible to split the equations of motion in three uncoupled subsets describing respectively the axial–torsional behavior, the in-plane motion and the out-of-plane motion of the array. The element co-ordinates can be split accordingly in three vectors:

$$\{\mathbf{Q}_{axltrs}\} = \begin{Bmatrix} Z_0 \\ \{\mathbf{q}_{w0}\} \\ \Phi_{z0} \\ \{\mathbf{q}_{v0}\} \end{Bmatrix}_{(10\times 1)}, \qquad \{\mathbf{Q}_{inp}\} = \begin{Bmatrix} X_0 + \mathrm{i}\,Y_0 \\ \{\mathbf{q}_{ux}\} + \mathrm{i}\{\mathbf{q}_{uy}\} \\ \{\mathbf{q}_{vx}\} + \mathrm{i}\{\mathbf{q}_{vy}\} \end{Bmatrix}_{(7\times 1)}$$

$$\{\mathbf{Q}_{outp}\} = \begin{Bmatrix} \Phi_{y0} - \mathrm{i}\Phi_{x0} \\ \{\mathbf{q}_{wy}\} - \mathrm{i}\{\mathbf{q}_{wx}\} \end{Bmatrix}_{(5\times 1)} \tag{31}$$

where $\mathrm{i} = \sqrt{-1}$ and besides each vector are indicated its dimensions. The notation adopted for the co-ordinates leads to a complex co-ordinate formulation of the corresponding equations of motion. Assuming that no external force acts on the element, the equations of motion are:

$$[\mathbf{M}_{axltrs}]\{\ddot{\mathbf{Q}}_{axltrs}\} + ([\mathbf{K}_{axltrs}] + \omega^2[\mathbf{K}_{axltrs\omega}] - \omega^2[\mathbf{M}_{niaxltrs}])\{\mathbf{Q}_{axltrs}\} = \{\mathbf{0}\}$$

$$[\mathbf{M}_{inp}]\{\ddot{\mathbf{Q}}_{inp}\} - \mathrm{i}\omega[\mathbf{G}_{inp}]\{\dot{\mathbf{Q}}_{inp}\} + ([\mathbf{K}_{inp}] + \omega^2[\mathbf{K}_{inp\omega}] - \omega^2[\mathbf{M}_{niinp}])\{\mathbf{Q}_{inp}\} = \{\mathbf{0}\}$$

$$[\mathbf{M}_{outp}]\{\ddot{\mathbf{Q}}_{outp}\} - \mathrm{i}\omega[\mathbf{G}_{outp}]\{\dot{\mathbf{Q}}_{outp}\} + ([\mathbf{K}_{outp}] + \omega^2[\mathbf{K}_{outp\omega}] - \omega^2[\mathbf{M}_{nioutp}])\{\mathbf{Q}_{outp}\} = \{\mathbf{0}\} \tag{32}$$

As in the case of the disc element [14], the terms $\omega^2[\mathbf{M}_{nij}]\{\mathbf{Q}_j\}$ account for the inertial forces acting on the element due to its deformation. They are due to the choice of referring the deformations of the element to a non-inertial frame.

Matrix $[\mathbf{G}_{inp}]$ accounts for the Coriolis forces acting on the blades when they are moving with speed $\{\dot{\mathbf{Q}}_{inp}\}$ on the plane of the array while matrix $[\mathbf{G}_{outp}]$ accounts for the gyroscopic forces due a motion of the inertial axes of the array with angular speed $\{\dot{\mathbf{Q}}_{outp}\}$.

Based on the partition of degrees of freedom of vectors (31) the explicit form of the element mass $[\mathbf{M}_i]$, gyroscopic $[\mathbf{G}_i]$ and non inertial matrices $[\mathbf{M}_{nii}]$ are:

$$[\mathbf{M}_{axltrs}] = \begin{bmatrix} m & [\mathbf{m}_{axl1}] & 0 & [\mathbf{0}] \\ [\mathbf{m}_{axl1}]^{\mathrm{T}} & [\mathbf{m}_{axl2}] & [\mathbf{0}] & [\mathbf{0}] \\ 0 & [\mathbf{0}] & J_p & [\mathbf{m}_{trs1}] \\ [\mathbf{0}] & [\mathbf{0}] & [\mathbf{m}_{trs1}]^{\mathrm{T}} & [\mathbf{m}_{trs2}] \end{bmatrix};$$

$$[\mathbf{M}_{outp}] = \begin{bmatrix} J_t & -[\mathbf{m}_{outp1}] \\ -[\mathbf{m}_{outp1}]^{\mathrm{T}} & [\mathbf{m}_{outp2}] \end{bmatrix};$$

$$[\mathbf{M}_{inp}] = \begin{bmatrix} m & [\mathbf{m}_{inp4}] & [\mathbf{m}_{inp5}] \\ [\mathbf{m}_{inp4}]^{\mathrm{T}} & [\mathbf{m}_{inp1}] & [\mathbf{0}] \\ [\mathbf{m}_{inp5}]^{\mathrm{T}} & [\mathbf{0}] & [\mathbf{m}_{inp2}] \end{bmatrix}; \qquad [\mathbf{G}_{outp}] = 2\begin{bmatrix} J_p/2 & -[\mathbf{m}_{outp1}] \\ -[\mathbf{m}_{outp1}]^{\mathrm{T}} & [\mathbf{m}_{outp2}] \end{bmatrix};$$

$$[\mathbf{G}_{inp}] = 2\begin{bmatrix} 0 & [\mathbf{0}] & [\mathbf{0}] \\ [\mathbf{0}] & [\mathbf{m}_{inp1}] & -[\mathbf{m}_{inp3}] \\ [\mathbf{0}] & -[\mathbf{m}_{inp3}]^{\mathrm{T}} & [\mathbf{m}_{inp2}] \end{bmatrix}; \qquad [\mathbf{M}_{niaxltrs}] = \begin{bmatrix} 0 & [\mathbf{0}] & 0 & [\mathbf{0}] \\ [\mathbf{0}] & [\mathbf{0}] & [\mathbf{0}] & [\mathbf{0}] \\ 0 & [\mathbf{0}] & 0 & [\mathbf{0}] \\ [\mathbf{0}] & [\mathbf{0}] & [\mathbf{0}] & [\mathbf{m}_{trs2}] \end{bmatrix};$$

$$[\mathbf{M}_{niinp}] = 2\begin{bmatrix} 0 & [\mathbf{0}] & [\mathbf{0}] \\ [\mathbf{0}] & [\mathbf{m}_{inp2}] & -[\mathbf{m}_{inp3}] \\ [\mathbf{0}] & -[\mathbf{m}_{inp3}]^{\mathrm{T}} & [\mathbf{m}_{inp2}] \end{bmatrix}; \qquad [\mathbf{M}_{nioutp}] = \begin{bmatrix} 0 & [\mathbf{0}] \\ [\mathbf{0}] & [\mathbf{m}_{outp2}] \end{bmatrix}. \tag{33}$$

The tangential displacements $\{\mathbf{q}_{t0}\}$ induce a change in the radius while the axial ones $\{\mathbf{q}_{w0}\}$ do not, this explains the term $[\mathbf{m}_{trs2}\}$ affecting only the torsional degree of freedom and not the tangential one in matrix $[\mathbf{M}_{niaxltrs}]$.

The stiffness matrices of equations (32) are partitioned as:

$$[\mathbf{K}_{axltrs}] = \begin{bmatrix} 0 & [\mathbf{0}] & 0 & [\mathbf{0}] \\ [\mathbf{0}] & [\mathbf{k}_{eaxltrs1}] & [\mathbf{0}] & [\mathbf{k}_{eaxltrs3}] \\ 0 & [\mathbf{0}] & 0 & [\mathbf{0}] \\ [\mathbf{0}] & [\mathbf{k}_{eaxltrs3}]^{\mathrm{T}} & [\mathbf{0}] & [\mathbf{k}_{eaxltrs3}] \end{bmatrix}; \qquad [\mathbf{K}_{outp}] = \begin{bmatrix} 0 & [\mathbf{0}] \\ [\mathbf{0}] & [\mathbf{k}_{eoutp}] \end{bmatrix};$$

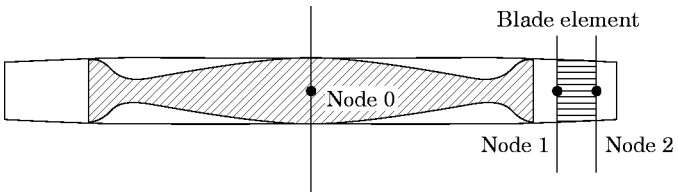

Figure 2. Element outline; 0 = central node common to all elements of the array, 1 = node at the inner radius of the element 2 = node at the outer radius.

$$[\mathbf{K}_{inp}] = \begin{bmatrix} 0 & [\mathbf{0}] & [\mathbf{0}] \\ [\mathbf{0}] & [\mathbf{k}_{einp1}] & [\mathbf{0}] \\ [\mathbf{0}] & [\mathbf{0}] & [\mathbf{k}_{einp2}] \end{bmatrix}; \qquad [\mathbf{K}_{inp\omega}] = \begin{bmatrix} 0 & [\mathbf{0}] & [\mathbf{0}] \\ [\mathbf{0}] & [\mathbf{0}] & [\mathbf{0}] \\ [\mathbf{0}] & [\mathbf{0}] & [\mathbf{k}_{ginp\omega}] \end{bmatrix};$$

$$[\mathbf{K}_{ax1trs\omega}] = \begin{bmatrix} 0 & [\mathbf{0}] & 0 & [\mathbf{0}] \\ [\mathbf{0}] & [\mathbf{k}_{gax1\omega}] & [\mathbf{0}] & [\mathbf{0}] \\ 0 & [\mathbf{0}] & 0 & [\mathbf{0}] \\ [\mathbf{0}] & [\mathbf{0}] & [\mathbf{0}] & [\mathbf{k}_{gtrs\omega}] \end{bmatrix}; \qquad [\mathbf{K}_{outp\omega}] = \begin{bmatrix} 0 & [\mathbf{0}] \\ [\mathbf{0}] & [\mathbf{k}_{goutp\omega}] \end{bmatrix}. \tag{34}$$

All square matrices of equations (33) and (34) are real and symmetric; their number of rows (and columns) is consistent with the dimensions of the vectors of the degrees of freedom which multiply them in the dynamic equation (32).

The expressions of the terms of these matrices are quite intricate and the analytical integration is difficult, particularly for what the geometric matrices are concerned. The element was implemented with a numeric integration routine, based on a four point Gauss procedure. Operating in this way the integration of the geometric matrices is straightforward.

5. DISC-ARRAY OF BLADES TRANSITION ELEMENT

The displacement field within the array of the blades element has been assumed to be due to the rigid body motion of its midplane and to the deviations from it. The co-ordinates employed to describe the deviations from the rigid body configuration include the displacements and rotations of nodes 1 and 2 of the element in-plane and out-of-plane of the array. These displacements are not compatible with the displacements of the beam elements that are used to model the shaft, as the formulation of these elements usually assumes that the sections remain plane during the deformation. Even if the displacements within the array of blades are very similar to those of the disc element [14], different kinds of shape functions have been adopted for the two, for the tangential displacements, i.e., linear shape functions have been chosen for the disc element while cubic ones for the array of blades. Two *transition elements* should then be developed to insure the compatibility of the displacement fields at the shaft-array of blades and at the disc-array of blades interfaces. Taking into account that the blades are seldom connected directly to a shaft, just the disc-array of blades transition element has been developed. This choice does not preclude the possibility of connecting an array to a shaft through a disc with a very small radial extension or, as a limiting case, to the outer node of a shaft–disc transition element with a vanishingly small radial extension.

The disc-array of blades transition element is provided with three nodes: nodes 0 and 2 are of the same type of node 0 and node 2 of the array of blades (Figure 2). The node at the center is connected directly with the shaft elements and coincides with the central node of all disc and blade elements used to model a disc-array subsystem at a given axial location.

Node 0 has two complex degrees of freedom for flexural behavior, one real degree of freedom for torsional and one for axial behavior. Node 2 has five complex degrees of freedom for flexural behavior, two real degrees of freedom for the torsional behavior and two real axial degrees of freedom.

The interface between the disc and the array is given by node 1 with four complex degrees of freedom for flexural behavior, one real degree of freedom for the torsional behavior and two real for the axial one. Its matrices have been obtained from those valid for the array of blade element by constraining the rotation about the tangential direction at node 1. Making reference to the symbols of equation (9) and taking into account of the assembly of the complex degrees of freedom of the element (31):

$$\beta_{vy1} - \mathrm{i}\beta_{vx1} = 0 \tag{35}$$

This is equivalent to the assumption that the blades remain perpendicular to the disc outer radius even if it is subject to a tangential displacement field.

In addition to the constraint equation (35) compatibility conditions must be included to make the degree of freedom of the node 1 of the transition element consistent with those of node 2 of the disc element. Taking into account that the out-of-plane deflections of the disc element at its node 2 are described in terms of complex rotation, $\varphi_{y2} - \mathrm{i}\varphi_{x2}$ about the y- and x-axis and that the tangential displacement are given in terms of rotation φ_{z2} about the z-axis, the compatibility conditions at the interface node between the disc and the transition element can be written as:

$$\varphi_{y2} - \mathrm{i}\varphi_{x2} = (w_{y1} - \mathrm{i}w_{x1})/r_i, \qquad \varphi_{z2} = v_{01}/r_i \tag{36}$$

where r_i is the inner radius of the transition element. The degrees of freedom to the left side of the equation (36) are relative to the outer node (2) of the disc element while those to the right are relative to the inner radius (1) of the transition element.

6. EXAMPLES

6.1. EXAMPLE 1: ROTATING PENDULUM

A rotating pendulum is a limit example for testing the inertial and centrifugal stiffening matrices of the present element. The natural frequencies of a rotating pendulum whose length is l, attached on a disc with radius r rotating at a speed ω are [14]

$$\lambda_1 = \omega\sqrt{1 + r/l}, \qquad \lambda_2 = \omega\sqrt{r/l} \tag{37}$$

respectively for oscillation in a plane for the axis of rotation and oscillation in a plane perpendicular to it.

A rotating pendulum is a good example of the symmetry breaking occurring in a reference frame rotating about a fixed axis. A heuristic explanation of this fact is shown in Figure 3: the linearized restoring force is $m\omega^2(r + l)\theta_2$ in the case of Figure 3a (oscillations in a plane containing the rotation axis) and $m\omega^2(r + l)(\theta_1 - \phi) \approx m\omega^2 r\theta_1$ in the case of Figure 3b (oscillations in a plane perpendicular to the rotation axis). It is also a good test of the present element in the sense that it implies using the element in conditions at the limits of its applicability: a mathematical pendulum, with a concentrated mass is badly modelled as a number of beam elements.

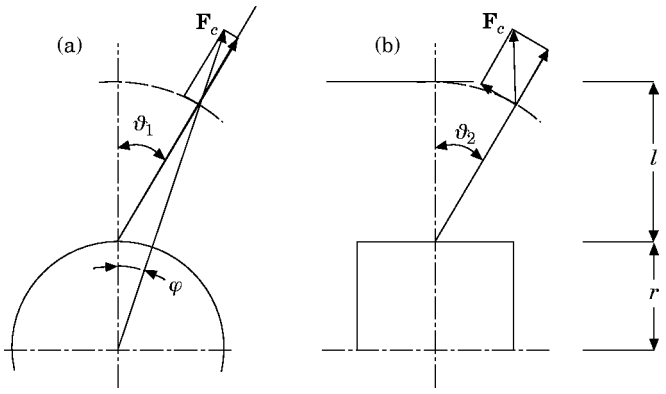

Figure 3. (a) In-plane and (b) out-of-plane oscillations of a rotating pendulum. Centrifugal force decomposed in its restoring and tensional components.

Owing to the last consideration, a fine mesh is required. A model consisting of two shaft elements, one shaft–disc transition element and one disc element, all of them very stiff, was built. The ends of the shaft element were constrained by rigid supports and also the axial displacement and the torsional rotation at one end were constrained. A row of 10 blades was then added, modelled by one transition element and 9 beam elements. The blades were assumed to be prismatic, with a cross-sectional area of 100 mm^2, and a Young's modulus of $2{\cdot}1 \times 10^{11}$ N/m^2 was assumed for all elements. A vanishingly small density of 0·01 kg/m^3 was assumed for all elements but the last one, for which a value of 4000 was used. The last element constitutes then the bob of the pendulum.

The inner radius of the transition element and the outer radius of the last blade element were assumed to be 200 and 402·5 mm respectively. The transition element was assumed to be very short, only 2 mm long, with area moments of inertia of 1×10^{-35} m^4: it constitutes then a sort of infinitely soft elastic point hinge. The last element is 5 mm long, its center of mass being located at a radius of 400 mm. The other elements are all equal, filling the space between the transition and the last element, their area moments of inertia are 1×10^{-9} m^4, angle $\psi = 0$. The resulting pendulum has then a length of 200 mm and a mass of 2 g. The computation was performed at a speed of 1000 rad/s. The exact frequencies of the pendulum are $\lambda_1 = 1000$ rad/s, $\lambda_2 = 1414$ rad/s, respectively for in-plane and out-of-plane oscillations.

By using a reduction scheme with 33 master degrees of freedom for the flexural behavior, 11 for the torsional and 11 for the axial behavior, the results shown in Table 1 have been

TABLE 1

Rotating pendulum. Torsional, axial and flexural natural frequencies at $\omega = 1000$ *rad/s computed through the present model and the closed form solution*

Harmonic		Present (rad/s)	Exact (rad/s)	Error (%)
in-plane 0		1012·67	1000·00	1·2
out-of-plane 0		1423·23	1414·21	0·6
in-plane 1	BWD	−12·67	0·00	–
	FWD	2012·67	2000·00	0·6
out-of-plane 1	BWD	−423·23	−414·21	2·2
	FWD	2423·23	2410·00	0·4

TABLE 2

Prismatic blade: *first five natural frequencies when stationary*; *in-plane vibrations of the blade with larger dimension in axial direction*. *The error is referred to the present model* 2 *compared with the closed form solution* (*the number of degrees of freedom is referred only to the master degrees of freedom*)

Frequency (Hz)	Closed form	FEM (22 d.o.f)	Present model 1 (7 d.o.f)	Present model 2 (14 d.o.f)	Error (%)
λ_1	399·93	399·98	399·98	399·98	0·013
λ_2	2506·53	2506·63	2507·52	2506·67	0·0056
λ_3	7019·06	7018·74	7039·79	7019·57	0·0073
λ_4	13754·86	13754·57	13948·69	13761·21	0·046
λ_5	22735·87	22739·62	22840·96	22771·99	0·16

obtained. The zero-harmonic component of the row of blades, i.e., the torsional and axial components, corresponds to the in-plane and out-of-plane oscillations of all pendulums occurring in phase. The first harmonic components are seen as flexural oscillations of the row, again corresponding to the in-plane and out-of-plane oscillations of all pendulums occurring out of phase. As seen in the case of the disc element [13], each oscillation mode generates two flexural modes, one backward and one forward, with frequencies $\lambda - \omega$ and $\lambda + \omega$.

The natural frequencies were computed at other values of the speed, obtaining a linear dependence as predicted by the theory. The present model yields results which are very close to the correct ones, particularly in the case of the out-of-plane modes, even in a case which is outside its immediate application limits.

6.2. EXAMPLE 2: SIMPLE PRISMATIC BLADE

A model consisting of a very stiff shaft (two shaft elements, as in the previous model) and a very stiff disc (one disc–shaft transition element and one disc element) was built. On the outer surface of the disc a row of 20 prismatic, untwisted blades with rectangular cross-section was added. The data for the blades are: inner radius 66 mm, length 64 mm, area and area moments of inertia of the cross section respectively 16 mm^2, 85·333 mm^4 and 5·333 mm^4, Young's modulus of 72×10^9 N/m^2, density 2800 kg/m^3, Poisson ratio 0·3. The row of blades was modelled using one blade–disc transition element and five blade elements (model 1). A second model with 12 blade elements was also built.

The blades were both located with the longer side in the axial and circumferential direction. The results obtained when stationary were compared with the closed form solution obtained in the literature for the Euler–Bernoulli beam. A conventional FEM model consisting of 10 Euler–Bernoulli beam elements was also computed in which the centrifugal force due to rotation was added using the geometric matrix approach. Note that this allows only computation of the out-of-plane zero-harmonic solution, i.e., the axial oscillations of the blade row.

The results obtained for the first five modes when stationary are reported in Tables 2 and 3. Note that even in the case of the fifth natural frequency the difference between the results obtained with the present model 2, using a reduction scheme with 14 master degrees of freedom, and the closed form solution is as small as 0·16%. The solution for the zero order harmonic (axial and torsional vibrations) coincides with that related to the first harmonic (lateral vibrations) with all the figures here reported.

TABLE 3

Prismatic blade: *Result for out-of-plane vibrations*; *details as for Table* 1

Frequency (Hz)	Closed form	FEM (22 d.o.f)	Present Model 1 (7 d.o.f)	Present model 2 (14 d.o.f)	Error (%)
λ_1	1599·74	1599·92	1599·93	1599·92	0·000
λ_2	10026·12	10026·53	10030·01	10026·68	0·0056
λ_3	28076·25	28074·98	28159·28	28078·41	0·0080
λ_4	55019·45	55018·29	55795·26	55045·36	0·047
λ_5	90943·48	90958·90	95365·14	91089·45	0·16

When the rotation of the bladed disc is accounted for, no closed form solution is available to compare the present results. It is however possible to compare the zero order harmonic out-of-plane frequencies (axial mode), with those computed using a standard FEM model based on beam elements in which centrifugal stiffening is accounted for using the geometric matrix (4). The results at 1500 and at 3000 rad/s for blades with the larger dimension laying in circumferential and axial direction are shown in Figure 4 and in Tables 4 and 5 respectively.

The fact that the error grows when the effect of the centrifugal stiffening is larger can be ascribed to the fact that in the control solution the centrifugal loading on the blade is accounted for in a rough way. To minimize these errors a very large number of beam elements have been used (100) but an even larger number would have given better results.

6.3. EXAMPLE 3: SHAFT WITH FLEXIBLE DISC AND BLADES

The simple rotor studied by Chun and Lee as model 1 in [3] was dealt with as a first bench-mark test. The rotor is the assembly of a shaft with circular cross-section and a bladed disc and is radially supported at its ends by rigid bearings. The eight untwisted blades have a constant rectangular cross-section with the longer side in circumferential direction. The shaft and the disc hub have been modelled using 12 beam elements with constant cross-section while one disc–shaft transition element and 4 disc elements have been used for the disc. The blades have been modelled using one disc-array transition element and 4 equally spaced blade elements. Displacement constraints have been introduced at the nodes were the bearings are located.

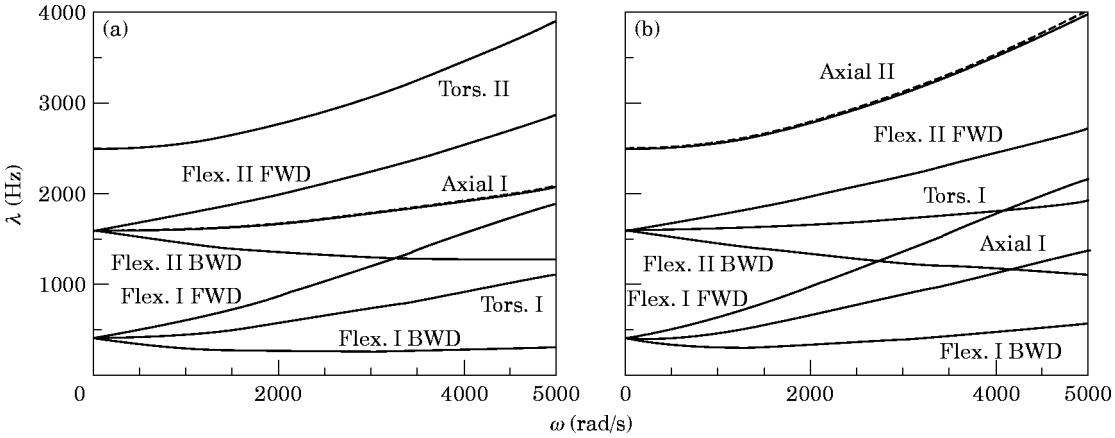

Figure 4. Natural frequencies of a row of blades with rectangular cross-section with the longer side in circumferential (a) and axial (b) direction as functions of the speed. Comparison between the present solution (——) and that obtained using beam elements (– – –).

TABLE 4

Prismatic blade: *first five natural frequencies at two different speeds*; *out-of-plane vibrations of the blade with larger dimension in circumferential direction*. *The error is referred to the present model* 2 *compared with the beam-element FEM solution* (*the number of degrees of freedom is referred only to the master degrees of freedom*)

	$\omega = 1500$ rad/s			$\omega = 3000$ rad/s		
Frequency (Hz)	FEM (202 d.o.f)	Present model 2 (14 d.o.f)	Error [%]	FEM (202 d.o.f)	Present model 2 (14 d.o.f)	Error [%]
λ_1	567·12	565·18	0·34	893·48	888·86	0·52
λ_2	2678·87	2675·80	0·11	3138·00	3127·12	0·35
λ_3	7195·76	7194·06	0·024	7699·53	7690·33	0·12
λ_4	13939·39	13944·49	0·037	14479·73	14477·50	0·015
λ_5	22927·00	22960·95	0·15	23489·43	23515·81	0·11

A Guyan reduction has been applied to decrease the dimensions of the model; 89 degrees of freedom describe the flexural behavior, 35 the torsional and 42 the axial behavior.

6.3.1. *Natural frequencies at standstill*

The first two natural frequencies computed with the present model at standstill are compared in Table 6 to the results reported in [3] and [15]. The higher discrepancies are related to the case of the assumed modes method. In all cases the results given by the present FEM model is within the same range of the FEM model of reference [15].

6.3.2. *Campbell diagram*

The Campbell's diagram for the first two forward and backward natural frequencies of the rotor is reported in Figure 5 as obtained by the present model along with the same

TABLE 5

Prismatic blade: *details as for Table* 4 *but results for larger dimensions in axial direction*

	$\omega = 1500$ rad/s			$\omega = 3000$ rad/s		
Frequency (Hz)	FEM (202 d.o.f)	Present model 2 (14 d.o.f)	Error [%]	FEM (22 d.o.f)	Present model 2 (14 d.o.f)	Error [%]
λ_1	1649·92	1649·24	0·041	1791·39	1788·88	0·14
λ_2	10070·98	10070·33	0·006	10203·21	10200·13	0·030
λ_3	28119·40	28122·60	0·011	28253·55	28254·70	0·004
λ_4	55061·62	55091·47	0·054	55201·63	55229·53	0·051
λ_5	90991·52	91136·78	0·16	91135·33	91278·61	0·16

TABLE 6

First two natural frequencies at standstill and critical speeds

Frequency (Hz)	Present FEM	Assumed modes method Ref. [3]	FEM Ref. [15]
λ_1	46·2	47·17	46·00
λ_2	61·6	59·92	60·15
Critical speed	47·59	47·78	46·11

diagram as reported by [3]. Although both methods give very close results where the first forward and second backward modes are concerned, the first backward and second forward modes obtained by the present model show a smaller (higher) dependence from the rotating speed than the assumed mode method in reference [3]. This can be ascribed to a larger centrifugal stiffening effect.

The last row of Table 6 shows that the values of the critical speed as computed by the present method are close to those computed by [3] and [15].

6.4. EXAMPLE 4: ROTOR OF A TURBOMOLECULAR PUMP RUNNING ON MAGNETIC BEARINGS

To show how the row-of-blades element performs when used in an actual environment, together with beam and disc elements, consider the case of a rotor of a turbomolecular pump running on magnetic bearings. The rotor has quite a complex geometry, as it includes 11 bladed discs plus a non-bladed one and a long shaft on which the laminations of the electric motor and of the bearing actuators and sensors are press-fit. A sketch of the model is shown in Figure 6. The statistics of the model are reported in Table 7, model 2. As the stagger angle of the blades is not vanishingly small (the blades are however not twisted), the axial behavior is coupled with the torsional one.

It must be explicitly noted that the previous examples were related to comparison between different numerical results while in the present case the comparison is with experimental ones in a very complex case. As a consequence of the uncertainty of many parameters and of many of the features of the model, the numerical results are expected to be far less close to the control ones than in the previous cases. Among the points which can detract from the precision of the results are the exact values of the Young's moduli, geometrical tolerances and the impossibility of accounting for complex interface conditions between the shaft and the laminations of the bearings, the sensors and the motor.

As the experimental values of the natural frequencies when stationary were available for the freely-suspended rotor, the computations were performed for the same condition. The results from a simpler model (Table 7, model 1) in which the discs and blades were modelled as rigid bodies were also available.

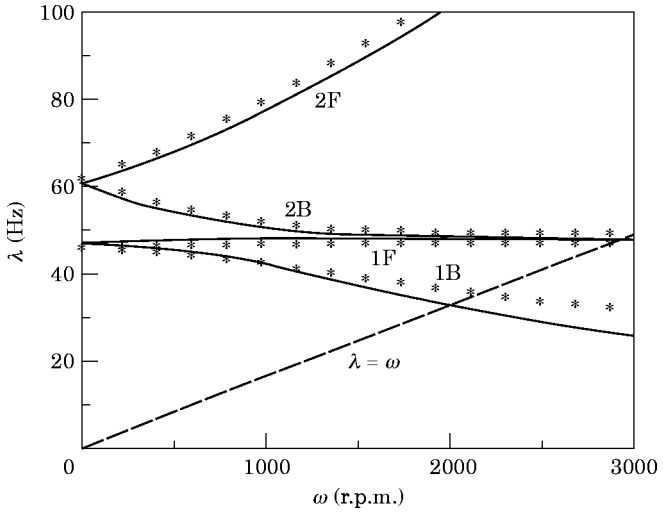

Figure 5. Example 3. Natural frequencies of model 1 (***) and Reference [3] (——).

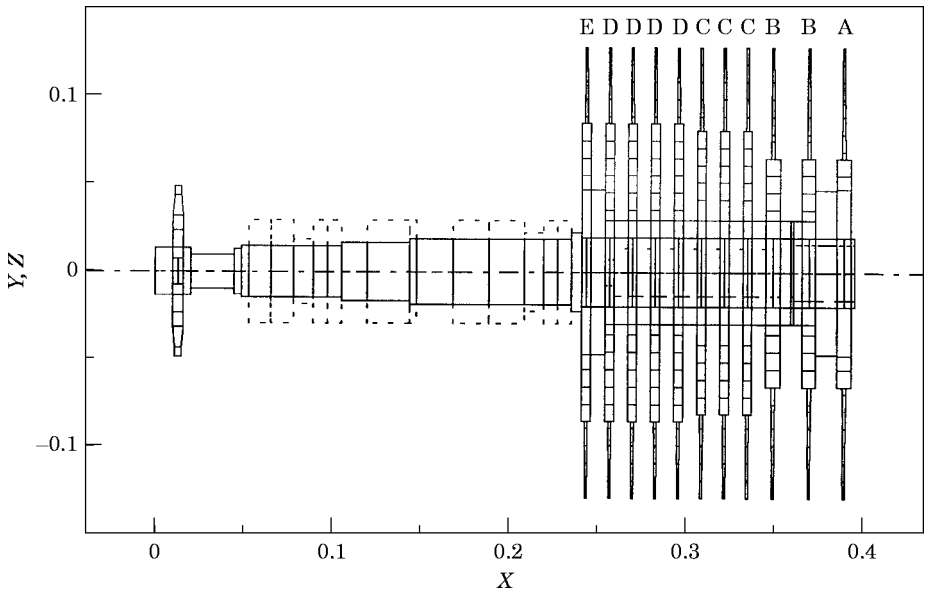

Figure 6. Example 4. Sketch of the model of the turbo molecular pump rotor.

The experimental tests were conducted using DIFA Measuring Systems dynamic signal analyzer DSA220-C, a PCB 086-B01 440 N instrumented hammer and PCB 353-B02 accelerometers. The flexural natural frequencies were measured by hanging the complete rotor with its axis held in a vertical direction using a thin steel wire. Five accelerometers were located at the sensor and actuator locations and between the first and second discs (A and B). For measuring the axial natural frequencies the rotor has been installed on the machine and magnetically levitated. An accelerometer was located at one end of the shaft, which was excited with the instrumented hammer at the opposite end.

6.4.1. *Natural frequencies when stationary*

The first 35 flexural natural frequencies (not included the two rigid-body modes) are reported in Table 8. The values obtained from the complete and simplified models are compared with the experimental ones. In the first case Guyan reduction was applied and a total of 249 master degrees of freedom was used.

TABLE 7

Statistics of the models for the turbomolecular pump rotor (*model* 1, *simplified model*; *model* 2, *complete model*)

		Elements						D.o.f.		
Model	Nodes	beam	mass	beam–disc transition	disc	disc–blade transition	blade	flexural	axial	torsional
1	33	32	16	–	–	–	–	66	33	33
2	188	66	–	12	57	11	53	697	567	

TABLE 8

Flexural natural frequencies when stationary. Simplified model (1), *complete model* (2) *and experimental values* (3). *The relative errors of the numerical results have been also reported*

$\omega = 0$ r.p.m.					
(1) (Hz)	(2) (Hz)	(3) (Hz)	Δ 1 − 3 (%)	Δ 2 − 3 (%)	Mode type
–	377	380	–	−0·8	first mode blades D, E
–	377	380	–	−0·8	first mode blades D, E
–	377	380	–	−0·8	first mode blades D, E
–	377	380	–	−0·8	first mode blades D, E
–	378	380	–	−0·5	first mode blades D, E
–	396	400	–	−1·0	first mode blades A, B
–	398	400	–	−0·5	first mode blades A, B
–	399	400	–	−0·3	first mode blades A, B
–	440	430	–	+2·3	first mode blades C
–	448	430	–	+4·2	first mode blades C
–	448	430	–	+4·2	first mode blades C
569	644	653	−12·9	−1·4	first mode rotor shaft
–	903	950	–	−4·9	first mode discs D, E
–	910	950	–	−4·2	first mode discs D, E
–	910	950	–	−4·2	first mode discs D, E
–	912	950	–	−4·0	first mode discs D, E
–	915	950	–	−3·7	first mode discs D, E
–	950	1059	–	−10·3	first mode discs C
–	951	1059	–	−10·2	first mode discs C
–	990	1059	–	−6·5	first mode discs C
1208	1275	1234	−2·1	+3·3	second mode rotor shaft
–	1445	1400	–	+3·2	first mode discs A, B
–	1452	1550	–	−6·3	first mode discs A, B
–	–	1659	–	–	first mode discs A, B
1948	1693	1744	10·5	−2·9	third mode rotor shaft
2851	2304	2222	28·3	−3·9	fourth mode rotor shaft
–	2695	2550	–	+5·7	second mode blades A, B
–	2706	2550	–	+6·1	second mode blades A, B
–	2759	2550	–	+8·2	second mode blades A, B
–	2864	2978	–	−3·8	second mode blades D, E
–	2866	2978	–	−3·8	second mode blades D, E
–	2866	2978	–	−3·7	second mode blades D, E
–	2867	2978	–	−3·7	second mode blades D, E
–	2868	2978	–	−3·7	second mode blades D, E
3844	3273	3125	23	+4·7	fifth mode rotor shaft

The first 32 coupled axial-torsional natural frequencies (not including the two rigid-body modes) are reported in Table 9. The values obtained from the complete model (with 376 master degrees of freedom) are compared with both the experimental ones and those obtained by modelling only the blades as beams clamped at one end.

The model based on rigid-body modelling of the bladed discs allows one to find only a limited number of the actual frequencies of the rotor, and even then leads to approximations which can be unacceptable. The precision with which the present model allows one to obtain the frequency of the first shaft mode is very remarkable (error of 1.4% against 13% of the simpler model). A very good accuracy is maintained also for the higher order modes.

The complexity of the model and the presence of several rows of identical blades leads to the presence of almost identical eigenvalues; the numerical model spreads out some of them, with a number of natural frequencies larger than those identified experimentally. However, the values obtained are very close to the measured ones. In the case of the coupled torsional–axial response, two of the numerical values could not be readily identified and do not correspond to any experimental value. Some difficulties can be due to the disc–shaft interface conditions: in some cases, e.g., the first disc B or the last disc D, the diameter at which the disc can be assumed to be clamped are different on the two sides, leading to modelling uncertainties. However, this seems not to affect the results as those for discs A and B are not worse than the others.

As a last remark, the mode shape for the seventh mode (the fifth if the rigid body modes are not included) for the coupled torsional–axial response is reported in Figure 7. The

TABLE 9

Coupled axial–torsional natural frequencies when stationary computed by modelling the single blades as clamped beams (1), *from the complete model* (2) *and measured experimentally* (3). *The relative errors of the numerical results have been also reported*

$\omega = 0$ r.p.m.					
(1) (Hz)	(2) (Hz)	(3) (Hz)	Δ 1 − 3 (%)	Δ 2 − 3 (%)	Mode type
429	378	380	12·9	−0·5	first mode blades D, E
429	378	380	12·9	−0·5	first mode blades D, E
429	378	380	12·9	−0·5	first mode blades D, E
429	378	380	12·9	−0·5	first mode blades D, E
429	382	380	12·9	+0·5	first mode blades D, E
406	391	400	1·5	−2·3	first mode blades A, B
406	391	400	1·5	−2·3	first mode blades A, B
406	403	400	1·5	+0·8	first mode blades A, B
541	447	430	25·8	+4·0	first mode blades C
541	447	430	25·8	+4·0	first mode blades C
541	460	430	25·8	+7·0	first mode blades C
–	932	940	–	−0·8	first mode dics D, E
–	943	940	–	+0·3	first mode discs D, E
–	943	940	–	+0·3	first mode discs D, E
–	944	940	–	+0·4	first mode discs D, E
–	945	940	–	+0·5	first mode discs D, E
–	971	1059	–	−8·3	first mode discs C
–	974	1059	–	−8·0	first mode discs C
–	1022	1059	–	−3·5	first mode discs C
–	1341	1537	–	−12·8	first mode discs A, B
–	1353	1537	–	−12·0	first mode discs A, B
–	1603	1659	–	−3·1	first mode discs A, B
–	2061	–	–	–	–
–	2335	–	–	–	–
2541	2422	2556	−0·6	−5·2	second mode blades A, B
2541	2446	2556	−0·6	−4·3	second mode blades A, B
2541	2517	2556	−0·6	−1·5	second mode blades A, B
2688	2655	2991	−10·1	−11·2	second mode blades D, E
2688	2721	2991	−10·1	−9·0	second mode blades D, E
2688	2744	2991	−10·1	−8·3	second mode blades D, E
2688	2757	2991	−10·1	−7·8	second mode blades D, E
2688	2775	2991	−10·1	−7·2	second mode blades D, E

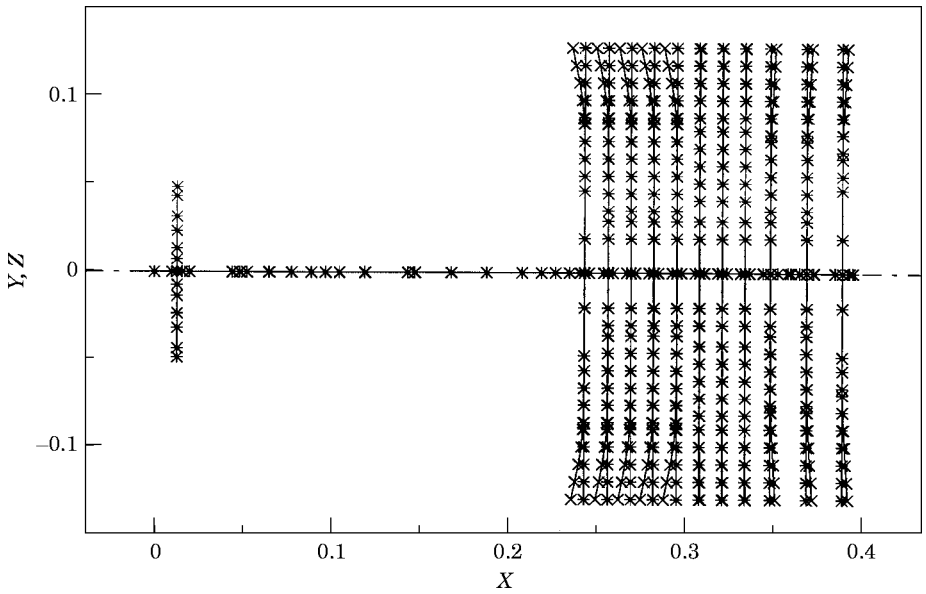

Figure 7. Example 4. Free–free mode shape for the seventh mode (the fifth if the rigid body modes are not included) for the coupled torsional–axial response: natural frequency 2405 rad/s (382·8 Hz) at $\omega = 0$.

mode was labelled as interesting as the blades of discs D and E, but from the figure it is clear that also those of discs A and B are affected.

6.4.2. *Critical speeds and Campbell diagram*

The first four critical speeds are reported in Table 10. The values obtained from the complete model (with 376 master degrees of freedom) are compared only with those obtained from the simplified model, as no experimental results were available.

The deformation of the discs and blades lowers the first critical speeds, although the effect on the first one is reasonably small, but does not introduce new critical speeds at rotational frequencies close to the natural frequencies of the blades at standstill. This is clearly to be ascribed to the strong centrifugal stiffening and to the gyroscopic effect, as also clear from the Campbell diagram for flexural modes shown in Figure 8.

TABLE 10

First four critical speeds computed from the complete model (2) *and the simplified model* (1). *The relative errors of simplified versus the complete model are also reported*

ω_{cr}		
(1) (r.p.m.)	(2) (r.p.m.)	Δ 1 − 2 (%)
53 600	48 274	11·0
134 090	111 930	19·8
276 170	202 905	36·1
441 199	289 384	52·5

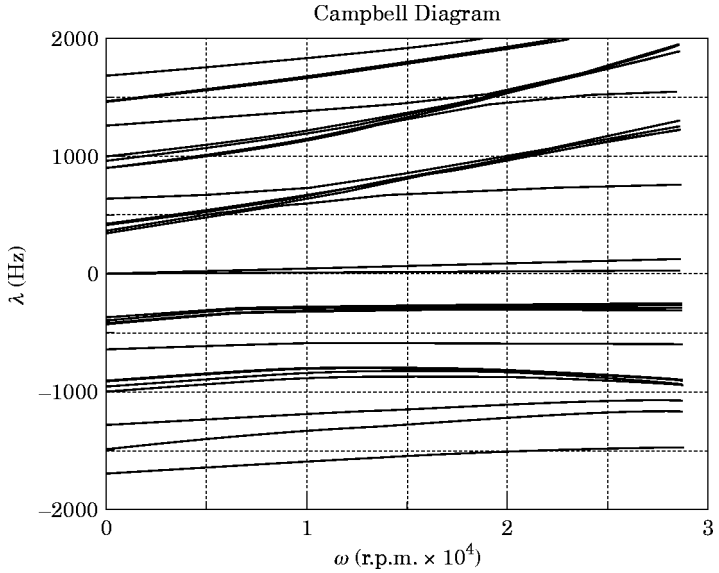

Figure 8. Example 4. Campbell diagram for flexural modes extended to the operating speed range.

7. CONCLUSIONS

A finite element aimed at modeling an array of blades for the study of their axial, torsional and flexural behavior has been developed. The displacement field within the element is approximated by trigonometrical expansion of the displacement field along the tangential direction and a polynomial expansion along the radius. Only the harmonics giving zero and one nodal diameter have been taken into account in the expansion as they are the only ones coupled to the dynamic behavior of the rotor. The element is provided with three nodes: two of them are located at the element inner and outer radii, their degrees of freedom are used to account for the deflections of the array out of the rigid body configuration while the degrees of freedom of the node lying on the element axis describe the rigid body motion.

The formulation has been obtained by following a Lagrangian approach which accounts for Coriolis and gyroscopic effects and stress stiffening. A constant stress contribution has not been considered as the blades are assumed to be unconstrained in the radial direction at their tip. This is consistent with the assumption that no connection exists between contiguous blades at the outer diameter such as shrouds, lacing wires or hoops.

As with the case of the disc element [13], the motion in the plane of the array and that out of it is shown to be decoupled while the axial and torsional motions are elastically coupled by the stagger and pretwist angles.

The element equations of motion are formulated in a complex co-ordinate formalism, which is consistent with the formulation of the FEM code (DYNROT) in which the element has been implemented. This allows an extension of the field of application of the DYNROT code to more complicated rotors which include bladed discs.

A disc-array of blades transition element has been developed to link the array of blades to the disc finite elements developed in [13]. It is based on the assumption that the blades are clamped to the disc at the inner radius of the array.

The analytical results that can be obtained in the cases of a rotating pendulum and rotating untwisted blades connected to a rigid disc and a rigid shaft have been compared to those given by the array of blades finite element showing in both cases a good agreement.

The experimental validation of the array of blades and of the disc finite element has been carried out on the rotor of a turbomolecular pump including 11 disc-array of blades assemblies. The values of the axial and the flexural natural frequencies predicted by the finite element model are shown to be in good agreement with the experimental results obtained when stationary, particularly when the modelling and general data uncertainty are considered. Compared to the geometric complexity of the rotor, its finite element model requires a reasonably small number of degrees of freedom while still preserving its accuracy.

ACKNOWLEDGMENTS

The Authors are grateful to Dr. Stefano Carabelli and Ing. Anolrea Argondizza for the experimental results regarding the turbomolecular pump.

REFERENCES

1. A. Leissa 1981 *Applied Mechanics Review* **34**, 629–635. Vibrational aspects of rotating turbomachinery blades.
2. E. F. Crawley and D. R. Mokadam 1984 *American Society of Mechanical Engineers Journal of Vibration*, *Acoustics*, *Stress and Reliability in Design* **106**, 181–188. Stagger angle dependence of inertial and elastic coupling in bladed discs.
3. S. B. Chun and C. W. Lee 1996 *Journal of Sound and Vibration* **189**, 587–608. Vibration analysis of shaft-bladed disc system by using substructure synthesis and assumed modes method.
4. T. Tomioka, Y. Kobayashi and G. Yamada 1996 *Journal of Sound and Vibration* **191**, 53–73. Analysis of free vibration of rotating disc-blade coupled systems by using artificial springs and orthogonal polynomials.
5. A. Zmitrowicz 1996 *Journal of Sound and Vibration* **192**, 521–533. A note on natural vibrations of turbine blade assemblies with non-continuous shroud rings.
6. J. Kirkhope and G. J. Wilson 1976 *Journal of Sound and Vibration* **49**, 469–482. A finite element analysis for the vibration modes of a bladed disc.
7. S. J. Wildheim 1983 *American Society of Mechanical Engineers Journal of Vibration*, *Acoustics*, *Stress and Reliability in Design* **105**, 416–424. Natural frequencies of rotating bladed discs using clamped–free blade modes.
8. P. J. Magari, L. A. Shultz and V. R. Murthy 1988 *Computer and Structures* **29**, 763–782. Dynamics of helicopter rotor blades.
9. P. J. Magari and L. A. Shultz 1987 *American Institute of Aeronautics and Astronautics Student Journal*, 17–27. Development of a rotating blade finite element with an application to the analysis of helicopter rotor systems.
10. M. Sakata, K. Kimura and S. K. Park 1989 *Journal of Sound and Vibration* **131**, 417–430. Vibration of bladed flexible rotor due to gyroscopic moment.
11. S. H. Hsieh and J. F. Abel 1995 *Journal of Sound and Vibration* **182**, 91–107. Comparison of two finite element approaches for analysis of rotating bladed-disc assemblies.
12. V. Omprakash and V. Ramamurti 1988 *Journal of Sound and Vibration* **125**, 357–366. Natural frequencies of bladed discs by a combined cyclic symmetry and Rayleigh-Ritz method.
13. G. Genta and A. Tonoli 1996 *Journal of Sound and Vibration* **196**, 19–43. A harmonic finite element for the analysis of flexural, torsional and axial rotordynamic behavior of discs.
14. G. Genta 1995 *Vibration of structures and machines*: *practical aspects*. New York: Springer; second edition.
15. W. Zhang, W. Wang and H. Wang 1996 *Proceedings of the Fourth International Conference on Rotor Dynamics*, 63–68. Analytical and experimental investigation of bladed-disk/shaft coupled system.

APPENDIX: NOMENCLATURE

J_p	inertia moment about the z-axis
J_t	inertia moment about the x- or y-axes
$[\mathbf{k}_{ei,j}]$, $[\mathbf{k}_{gi,\omega}]$	$i = axl$, trs, inp, $outp$, $j = 1, 2$ stiffness sub-matrices
l	length of rotating pendulum
$[\mathbf{m}_{i,j}]$	i = axl, trs, inp, $outp$, j = 1, 2 mass sub-matrices
$[\mathbf{n}_u(\chi)]$	shape functions for radial displacements
$[\mathbf{n}_v(\chi)]$	shape functions for tangential displacements
$[\mathbf{n}_w(\chi)]$	shape functions for axial displacements
$\{\mathbf{q}_{t0}\}$, $\{\mathbf{q}_{w0}\}$	torsional and axial degrees of freedom
$\{\mathbf{q}_{ux}(t)\}$, $\{\mathbf{q}_{uy}(t)\}$	element radial degrees of freedom
$\{\mathbf{q}_{vx}(t)\}$, $\{\mathbf{q}_{vy}(t)\}$	element tangential degrees of freedom
$\{\mathbf{q}_{wx}(t)\}$, $\{\mathbf{q}_{wy}(t)\}$	element axial degrees of freedom
$\{\mathbf{r}\}$	undeformed location of point P_i in rotating polar co-ordinates
$\{\mathbf{s}\}$	displacement of point P_i in rotating polar co-ordinates
r	radial co-ordinate
r_i, r_o	inner and outer radii of the element
t	time
u, v, w	radial, tangential and axial displacements
u_1, u_2, u_3	principal area inertial axes of a blade section
w_0	zero harmonic coefficient function (axial)
v_0	zero harmonic coefficient function (tangential)
u_x, u_y	first harmonic coefficient functions (radial)
w_x, w_y	first harmonic coefficient functions (axial)
v_x, v_y	first harmonic coefficient functions (tangential)
A, B, C, D	components of $[n_v(\chi)]$ and $[n_w(\chi)]$ shape functions
$A(\chi)$	area of blade cross-section at non-dimensional radius χ
$\{\mathbf{C}\}$	co-ordinate vector of point C
F_r	radial force
$[\mathbf{G}_i]$	gyroscopic matrices
I_2, I_3	area moments of inertia of a blade about u_2 and u_3 directions
$[\mathbf{K}_i]$	stiffness matrices
$[\mathbf{K}_{\omega i}]$	geometric stiffness matrices
L	Lagrangian function
$[\mathbf{M}_i]$	i = axl, trs, inp, outp mass matrices
$[\mathbf{M}_{nii}]$	i = inp, outp non inertial mass matrices
N	number of blades
$P_{r\omega}$	radial force per unit ω
$\{\mathbf{P}_i\}$	co-ordinate vector of a point P
$\{\mathbf{Q}_i\}$	element complex degrees of freedom
$[\mathbf{R}_i]$	rigid body rotation matrices
T	kinetic energy
U	potential energy
U_e, U_g	elastic and geometric potential energies
$\beta_{v,w}$	radial derivatives of w and v displacements
χ	non-dimensional radial co-ordinate
$\lambda_{1,2}$	natural frequencies of a rotating pendulum
ϕ_0	torsional deformation
ϑ_i	angular location of a cross-section of the ith blade
ψ	angle between the w and u_2 directions
ρ	mass density
ω	rotating speed of the shaft
Δr	$\Delta r = r_o + r_i$
$\Phi_{X'}$	rigid body rotation of the disc about X'-axis
Φ_y	rigid body rotation of the disc about y-axis
Φ_z	rigid body torsional co-ordinate

Subscript

inp	in the plane of the disc
outp	out of the plane of the disc

axl	axial component
trs	torsional component
e	elastic component
g	geometric component
r	radial
i	*i*th-blade
c	circumferential
0, 1, 2	zero, first and second order contributions